# Integration of Active Nickel Oxide Clusters by Amino Acids for Water Oxidation

Masaaki Yoshida,[*,†,‡,§] Sho Onishi,[†,§] Yosuke Mitsutomi,[†] Futaba Yamamoto,[†] Masanari Nagasaka,[#] Hayato Yuzawa,[#] Nobuhiro Kosugi,[#] and Hiroshi Kondoh[†]

†Department of Chemistry, Keio University, Yokohama 223-8522, Japan
‡Cooperative Research Fellow, Institute for Catalysis, Hokkaido University, Hokkaido 060-0808, Japan
#Institute for Molecular Science, Myodaiji, Okazaki 444-8585, Japan

Ⓢ Supporting Information

**ABSTRACT:** The move toward sustainable hydrogen production from water using renewable energy, a highly efficient oxygen evolution electrocatalyst, is crucial because water-splitting efficiency is restricted to the oxygen evolution capability, which is insufficient compared to the hydrogen evolution reaction. Herein, we report a new method that improves the oxygen evolution activity by integration of active nickel oxide clusters using amino acids, meaning that the amount of electrodeposited nickel oxides is increasing with maintaining the catalytic activity. This method enhances the catalytic activity because the reaction sites drastically increase in three dimensions. The detailed reaction mechanism was investigated using operando UV/vis absorption and Ni K-edge X-ray absorption spectroscopic techniques, which suggested that amino acids such as glycine, alanine, and glutamine promoted the electrodeposition of $NiO_6$ octahedral structure clusters. Meanwhile, the analysis of N and O K-edge X-ray absorption spectra showed that the amino acid (glycine) in the nickel electrocatalyst was present in the molecular state. Therefore, it was spectroscopically demonstrated that amino acids are bound to nickel oxide clusters accompanied by oxygen evolution activity.
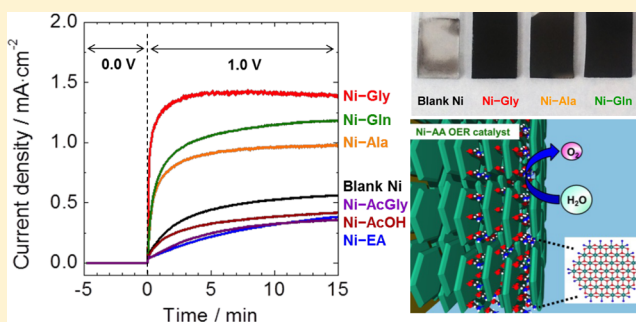
## 1. INTRODUCTION

Electrochemical water splitting using renewable non-fossil fuel energy sources such as sunlight, wind, and tides is a fascinating candidate for hydrogen production toward a sustainable society.[1−6] This reaction consists of two half reactions of hydrogen ($2H^+ + 2e^- \rightarrow H_2$) and oxygen ($2H_2O \rightarrow O_2 + 4H^+ + 4e^-$) evolution. However, the efficiency of the oxygen evolution reaction (OER) on general electrode materials is insufficient to develop a commercial water-splitting system due to the high overpotentials required to extract oxygen atoms from water molecules.[5−10] Therefore, the development of efficient OER electrocatalysts has received the most attention owing to the potential toward highly efficient hydrogen production.[5−28]

Generally, transition-metal oxides, such as $MnO_x$,[7−10] $CoO_x$[11−17] and $NiO_x$[18−21] are known to function as efficient OER electrocatalysts. Thus, substantial efforts have been made to develop OER electrocatalysts for improvement of the water oxidation efficiency. For example, Nocera and colleagues reported that cobalt−phosphate electrodeposited from a dilute $Co^{2+}$ solution in a phosphate-buffered electrolyte ($Co−P_i$) functions as an efficient OER electrocatalyst,[11−14] as do similar materials of cobalt−borate ($Co−B_i$)[11,13] and nickel−borate ($Ni−B_i$)[18−21] complexes. Meanwhile, it was recently reported

that the addition of certain organic molecules to metal oxide catalysts enhanced the OER activity.[22−28] Singh et al. and Hoang et al. proposed that the addition of diaminoethane, 3,5-diamino-1,2,4-triazole, or its derivatives to the $Ni^{2+}$ solution in a borate-buffered electrolyte enhanced the catalytic activity for water oxidation because of the difference in film morphology.[22−24] Moreover, Allen et al. suggested the enhancement of OER activity for $NiO_x$ electrocatalysts by amino acids (Ni−AA), and concluded that the presence of primary amines and phosphate is the key to the formation of the catalytically active nickel hydroxide species.[24] These OER catalysts are composed of inexpensive and earth-abundant materials and operate safely with high activity. However, the exploration of more efficient catalysts is still imperative to attain sustainable hydrogen production.

The reaction rate of transition-metal oxides is not sufficiently high, although the water oxidation reaction proceeds at a small overpotential.[6] Thus, increasing the reaction sites is the key to drastically enhancing the water oxidation efficiency. To increase the surface area of catalysts, various strategies have been applied
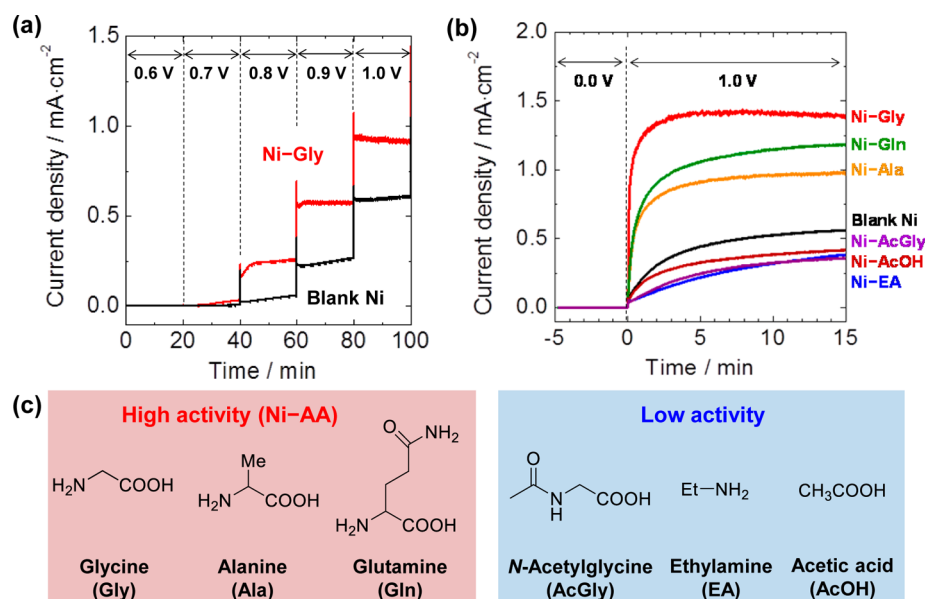
**Figure 1.** (a) OER current densities at various electrode potentials and (b) time courses of the OER current densities for blank Ni (black), Ni−Gly (red), Ni−Ala (orange), Ni−Gln (green), Ni−AcGly (purple), Ni−EA (blue), and Ni−AcOH (brown) catalysts on the ITO substrates in a K−P$_i$ buffer of pH 11 containing Ni(NO$_3$)$_2$ and molecular compounds. (c) Schematic models for molecular compounds.

for development of the nanoparticle assemblies.[29−35] For example, the Nishihara group reported that Pd nanoparticle assemblies can be formed using an organic linker with a rigid tetrahedral core.[34] Meanwhile, Martis et al. reported that Pd nanoparticles can be immobilized within the pores of metal−organic frameworks (MOF).[35] In such a situation, it was recently proposed that some OER electrocatalysts such as Co−P$_i$, Co−B$_i$, and Ni−B$_i$ are formed by assembly of nanosized clusters of transition-metal oxides.[11,17,19] The unique characteristics of these assemblies enable utilization of the thin film inside for water oxidation sites because the proton-coupled electron hopping proceeds within the bulk hydrated oxide films.[14,15,20] Therefore, an assembly technique to efficiently utilize the catalyst inside is of critical importance to develop three-dimensional (3D) functional materials with many reaction sites.

Here, we successfully demonstrated that amino acids integrate nickel oxide clusters in the Ni−AA electrocatalysts to drastically increase the number of reaction sites for OER activity. Operando observation under catalysis using differential UV/vis absorption and Ni K-edge X-ray absorption fine structure (XAFS) measurements supported the proposal concerning integration of nickel oxide clusters because the electrodeposition of nickel oxide species with the NiO$_6$ structure was promoted by amino acids. N and O K-edge XAFS spectra also implied that the nitrogen and oxygen species of the amino acid (glycine) in the nickel electrocatalyst were present in a similar chemical state as the isolated amino acid molecule. In this report, we discuss the detailed mechanism for the water oxidation reaction.

## 2. EXPERIMENTAL SECTION

A Teflon electrochemical cell was equipped with a Pt wire counter electrode and a Ag/AgCl (saturated KCl) reference electrode for all electrochemical experiments. Ni-AA thin films were electrodeposited on an indium tin oxide (ITO) or a Au thin film by controlled potential electrolysis at 1.0 V in a 0.1 M potassium phosphate (K−P$_i$) aqueous electrolyte of pH 11

containing 0.4 mM Ni(NO$_3$)$_2$ and 1.6 mM amino acids (Ni−AA) such as glycine (Ni−Gly), alanine (Ni−Ala), and glutamine (Ni−Gln) (none: blank Ni). To compare with other molecular compounds, ethylamine (Ni−EA), acetylglycine (Ni−AcGly), and acetic acid (Ni−AcOH) were also used instead of amino acids. The prepared Ni−Gly sample was analyzed using scanning electron microscopy (SEM), X-ray photoelectron spectroscopy (XPS), and a surface profilometer, confirming that the substrate was totally covered with Ni−Gly at a film thickness of ca. 100 nm with elemental composition of Ni, N, K, and P (Figures S1−S3 of the Supporting Information).

Operando differential UV/vis absorption spectra were obtained in diffuse transmission mode using a UV/vis spectrometer, according to previous work.[36] The operando Ni K-edge XAFS spectra were obtained in fluorescence mode at BL-9A in the Photon Factory (PF) and at BL01B1 in the SPring-8 facility, in accordance with previous work.[37] Soft X-ray XAFS measurements were performed in the total electron yield mode at the BL3U of the UVSOR Synchrotron and in the fluorescence yield mode at the BL-7A in the PF. Additional experimental details are included in the Supporting Information.

## 3. RESULTS AND DISCUSSION

Time courses of current densities for Ni−Gly in a K−P$_i$ aqueous electrolyte containing Ni(NO$_3$)$_2$ and glycine are shown in Figure 1a. The OER current of Ni−Gly was higher than that of the blank Ni at all electrode potentials, which indicates that the glycine molecule enhances the catalytic OER activity, as previously reported.[25] Moreover, the OER currents of Ni−Ala, Ni−Gln, and Ni−Gly also increased (Figure 1b), indicating that amino acids in the Ni−AA improve the OER activity. Considering that the currents of Ni−EA, Ni−AcGly, and Ni−AcOH were almost the same as that of blank Ni, the presence of NH$_2$ and COOH groups in the amino acids is the key for the enhancement of OER activity (Figure 1c). The OER current was maintained for at least 3 h, indicating that the
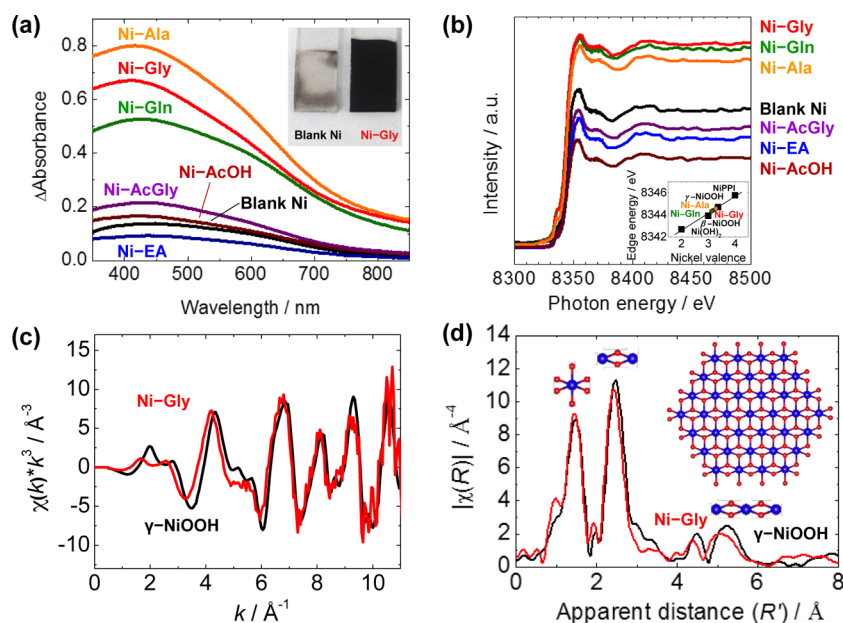
**Figure 2.** Operando (a) differential UV/vis absorption against 0.0 V of reference electrode voltage (inset: photographic images (see Figure S6)) and (b) Ni K-edge XAFS spectra (inset: estimation of nickel valence state using half edge energy (NiPPI: nickel potassium paraperiodate)) after 1 h maintained at 1.0 V in a K−P$_i$ buffer of pH 11 containing Ni(NO$_3$)$_2$ and various molecular compounds. (c) $k^3$-weighted and (d) FT EXAFS spectra of $\gamma$-NiOOH powder (black) and Ni−Gly (red) catalysts maintained at 1.0 V.

Ni−AA catalysts can function as stable OER catalysts (Figure S4). The differential molar amount of the oxidation reaction estimated from the differential currents between Ni−Gly and blank Ni catalysts for 3 h (ca. 74 $\mu$mol) was markedly higher than those of nickel ion (ca. 8 $\mu$mol) and glycine molecule (ca. 32 $\mu$mol) in the initial electrolyte solution, confirming that OER on the Ni−AA catalysts proceeded catalytically without the decomposition of glycine by the electrode potential. The Faradaic efficiency for the Ni−Gly catalyst during steady state was estimated to be ca. 96%, as shown in Figure S5, meaning that the observed oxidation currents for the Ni−AA catalysts are almost all used for the OER process.

Figure 2a shows the operando differential UV/vis absorption spectra at 1.0 V for 1 h in a 0.1 M K−P$_i$ electrolyte containing Ni(NO$_3$)$_2$ and various molecular compounds. A broad absorption peak was observed for all samples, indicating that nickel oxide species (probably NiOOH, see below) were electrodeposited on the ITO substrates. The peak intensities of UV/vis absorption spectra for Ni−Gly, Ni−Ala, and Ni−Gln were considerably higher than those of Ni−AcGly, Ni−EA, Ni−AcOH, and blank Ni samples. These results suggest that the electrodeposition of the samples proceeded for the Ni−AA samples but did not proceed for the other samples. This can be confirmed by the photographic image of Ni−AA electrocatalysts, as shown in Figure S6. Similar results by electrochemical quartz crystal microbalance (EQCM) are obtained for nickel and copper oxide films using glycine molecule as a semiconductor and electrochromic material by Ogura et al.[38−40] The same behavior in UV/vis absorption spectra was observed for the operando Ni K-edge XAFS measurements, as shown in Figure 2b. Considering that XAFS intensity is generally related to the abundance of the target element, it is concluded that amino acids integrate the NiO$_6$ clusters in the Ni−AA using nickel ion in the electrolyte. The OER activity increased little by little upon increasing the film thickness, indicating that the OER reaction proceeds not only at the

electrode surface but also in the thin film inside as 3D assembled electrocatalysts (Figure S7), as described previously.[14,15,20] The average nickel valences were roughly estimated to be ca. +3.1 to +3.3 for Ni−AA from the half edge energies of nickel reference samples, similar to those of $\beta$-NiOOH (Ni$^{3.0+}$) and $\gamma$-NiOOH (Ni$^{3.6+}$) materials (inset of Figure 2b).

To investigate the local structure of Ni species in the Ni−Gly, extended X-ray absorption fine structure (EXAFS) spectra were taken for the Ni−Gly sample as shown in Figure 2c, together with the $\gamma$-NiOOH powder reference. The first (Ni−O) and second (Ni−Ni) peaks for Ni−Gly were observed at the same peak position and intensity as those of the $\gamma$-NiOOH reference (Figure 2d), which showed that the local structure of Ni species in the Ni−Gly was composed of an edge-sharing NiO$_6$ octahedral ($\gamma$-NiOOH) structure. In similar work, the nickel species in the Ni−B$_i$ electrocatalyst at higher potential has been reported to be a nanosized NiO$_6$ cluster[18,19] because the second peak (Ni−Ni) intensity for Ni−B$_i$ was weaker than that for $\gamma$-NiOOH and no peak was observed above 3 Å in the EXAFS spectra. However, in this study, considering that all peak intensities for Ni−O and Ni−Ni bonds of Ni−Gly were the same as those for $\gamma$-NiOOH, the NiO$_6$ cluster is likely to be over a few nanometers in size. The SEM image of Ni−Gly suggests that the NiO$_6$ clusters are a few hundred nanometers in size (Figure S1).

The XAFS technique using soft X-rays is a powerful tool to investigate electronic states composed of light elements such as C, N, and O species.[41] Recently, we reported that NiO$_6$ octahedral domains in Ni−B$_i$ can be detected by O K-edge XAFS.[42] Thus, to learn about the glycine molecule, we observed N and O K-edge XAFS spectra for Ni−Gly under ultrahigh vacuum using fluorescence and electron yield modes, together with those for glycine and NiOOH (Figure 3). In the N K-edge XAFS spectrum using the electron yield mode, two peaks associated with nitrogen species were observed at ca.
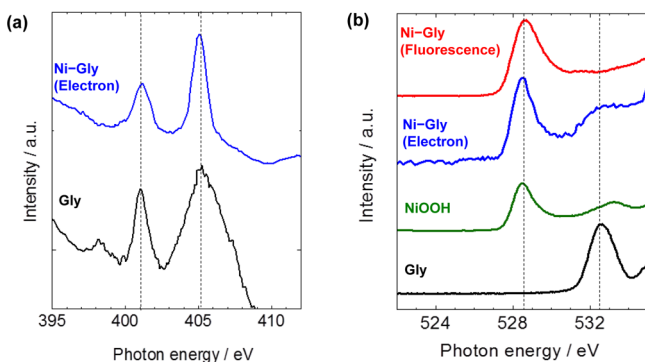
**Figure 3.** (a) N K-edge and (b) O K-edge XAFS spectra for the Ni—Gly electrocatalyst. It should be noted that the N K-edge XAFS spectrum for glycine molecule with electron yield mode was slightly distorted by the charge-up effect.

401.0 and 405.2 eV for Ni—Gly, which were similar to those in the glycine molecule reference and previous work,[43] indicating that Ni—Gly includes the glycine molecule. In the O K-edge XAFS measurements using the electron yield mode, two peaks were observed at ca. 528.6 eV for NiOOH and 532.4 eV for glycine. The presence of glycine molecule is likely to contribute to the combination with each $NiO_6$ cluster by binding with $NH_2$ and COOH groups. However, although the glycine species was also observed by X-ray photoelectron spectroscopy (XPS) measurements (Figure S3), it was not observed by XAFS using fluorescence yield (Figure 3) mode and X-ray fluorescence analysis (Figure S8), indicating that the glycine (amino acid) molecule is present only near the electrode surface (typically within 10 nm) of the OER thin film. On the basis of the XPS results of nickel and nitrogen species, the atomic ratio of Ni:N was ca. 10:3, indicating that several glycine molecules are likely to cover the $NiO_6$ clusters near the electrode surface.

Figure 4 shows a schematic model for the electrodeposition and water oxidation of the Ni—AA electrocatalyst. The positive potential supply to the Au electrode results in generation of Ni—AA with a $NiO_6$ cluster of octahedral structure by the electrodeposition of nickel ion in the electrolyte (Figure 4a). The amino acid combines the $NiO_6$ clusters by binding with $NH_2$ and COOH groups accompanied by OER activity. In contrast, molecular compounds without $NH_2$ and COOH groups did not exhibit the binding function between nanoclusters. Although the mechanism of catalyst assembly is under

investigation, it is likely to be related to complex formation between Ni ion and amino acids in the electrolyte solution (Figure S9). From some previous reports, the domain edge of $NiO_6$ octahedra is known to function as an active water oxidation site.[20,41] Therefore, we believe that the integration of $NiO_6$ octahedral clusters increases and extends the number of reaction sites for OER to three dimensions. The Ni—AA is likely to function not only at the electrode surface but also in the thin film inside as a 3D assembled electrocatalyst (Figure 4b), as described in similar work.[14,15,20] Further investigation is in progress.

Transition-metal oxides such as $MnO_x$, $CoO_x$, and $NiO_x$ are generally considered to exhibit high OER activity.[5−28] However, there is a disadvantage that OER current density is low in spite of the small overvoltage, compared with Pt electrodes. Our present technique shows that 3D assemblies of transition-metal oxides using amino acids are fascinating candidates to drastically increase the amount of reaction sites. This method is applied not only to amino acids but also to some other organic molecules. (Further investigation is in process.). The assembly technique of OER materials discovered by this study has provided the first successful proof-of-concept and there is the potential for it to be applied to many other OER electrocatalysts composed of transition-metal oxides such as $MnO_x$, $CoO_x$, and $NiO_x$ to increase the reaction sites for the OER process. The knowledge obtained here will be useful to develop more efficient OER catalysts toward sustainable water-splitting systems.

In conclusion, the function of amino acids was investigated by several spectroscopic techniques. Operando differential UV/vis absorption spectroscopy showed that the amino acids function to increase the amount of electrodeposited nickel species on the electrode surface. The result of operando Ni K-edge XAFS measurements showed that the local structure of the nickel species was composed of $NiO_6$ (NiOOH). Moreover, the observation of N and O K-edge XAFS suggested that the amino acid (glycine) in the nickel electrocatalyst maintained a similar chemical state with the amino acid molecule. On the basis of these studies, it was demonstrated that each nickel oxide cluster is combined with amino acids and the integration of active nickel oxide clusters is attained with a large amount of interface area between nickel oxide clusters and water molecules, accompanied by highly efficient OER activity.
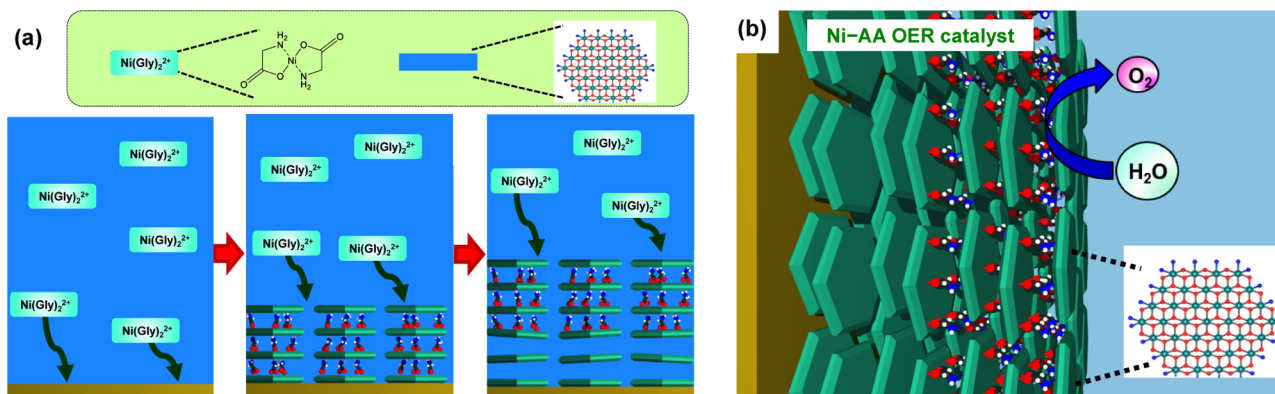


**Figure 4.** Proposed schematic model of (a) the formation of the Ni—AA electrocatalyst and (b) the water oxidation reaction processes. Nickel ion was integrated as active nickel oxide clusters by amino acids for water oxidation catalysis.

## ASSOCIATED CONTENT

**Ⓢ Supporting Information**

The Supporting Information is available free of charge on the ACS Publications website at DOI: 10.1021/acs.jpcc.6b08796.

> Detailed experimental procedures, SEM images, film thickness, XPS spectra, stability of catalyst, detection of evolved gas, photographic image, relationship between film thickness and catalysis, X-ray fluorescence, and nickel complex with glycine molecule (PDF)

## AUTHOR INFORMATION

**Corresponding Author**

*Tel.: +81-45-566-1592. Fax: +81-45-566-1697. E-mail: yoshida@chem.keio.ac.jp.

**ORCID**

Masaaki Yoshida: 0000-0002-3656-4444

**Author Contributions**

§These authors contributed equally.

**Notes**

The authors declare no competing financial interest.

## ACKNOWLEDGMENTS

## REFERENCES

(1) Christopher, K.; Dimitrios, R. A Review on Energy Comparison of Hydrogen Production Methods from Renewable Energy Sources. *Energy Environ. Sci.* **2012**, *5*, 6640−6651.

(2) Dincer, I.; Acar, C. Review and Evaluation of Hydrogen Production Methods for Better Sustainability. *Int. J. Hydrogen Energy* **2015**, *40*, 11094−11111.

(3) Tachibana, Y.; Vayssieres, L.; Durrant, J. R. Artificial Photosynthesis for Solar Water-splitting. *Nat. Photonics* **2012**, *6*, 511−518.

(4) Hisatomi, T.; Kubota, J.; Domen, K. Recent Advances in Semiconductors for Photocatalytic and Photoelectrochemical Water Splitting. *Chem. Soc. Rev.* **2014**, *43*, 7520−7535.

(5) Nocera, D. G. The Artificial Leaf. *Acc. Chem. Res.* **2012**, *45*, 767−776.

(6) Walter, M. G.; Warren, E. L.; McKone, J. R.; Boettcher, S. W.; Mi, Q.; Santori, E. A.; Lewis, N. S. Solar Water Splitting Cells. *Chem. Rev.* **2010**, *110*, 6446−6473.

(7) Najafpour, M. M.; Renger, G.; Hołyńska, M.; Moghaddam, A. N.; Aro, E.-M.; Carpentier, R.; Nishihara, H.; Eaton-Rye, J. J.; Shen, J.-R.; Allakhverdiev, S. I. Manganese Compounds as Water-Oxidizing Catalysts: From the Natural Water-Oxidizing Complex to Nanosized Manganese Oxide Structures. *Chem. Rev.* **2016**, *116*, 2886−2936.

(8) Robinson, D. M.; Go, Y. B.; Mui, M.; Gardner, G.; Zhang, Z.; Mastrogiovanni, D.; Garfunkel, E.; Li, J.; Greenblatt, M.; Dismukes, G. C. Photochemical Water Oxidation by Crystalline Polymorphs of Manganese Oxides: Structural Requirements for Catalysis. *J. Am. Chem. Soc.* **2013**, *135*, 3494−3501.

(9) Huynh, M.; Bediako, D. K.; Nocera, D. G. Functionally Stable Manganese Oxide Oxygen Evolution Catalyst in Acid. *J. Am. Chem. Soc.* **2014**, *136*, 6002−6010.

(10) Huynh, M.; Shi, C.; Billinge, S. J. L.; Nocera, D. G. Nature of Activated Manganese Oxide for Oxygen Evolution. *J. Am. Chem. Soc.* **2015**, *137*, 14887−14904.

(11) Bediako, D. K.; Ullman, A. M.; Nocera, D. G. Catalytic Oxygen Evolution by Cobalt Oxido Thin Films. *Top. Curr. Chem.* **2015**, *371*, 173−213.

(12) Kanan, M. W.; Nocera, D. G. In Situ Formation of an Oxygen-Evolving Catalyst in Neutral Water Containing Phosphate and Co$^{2+}$. *Science* **2008**, *321*, 1072−1075.

(13) Surendranath, Y.; Dincă, M.; Nocera, D. G. Electrolyte-Dependent Electrosynthesis and Activity of Cobalt-Based Water Oxidation Catalysts. *J. Am. Chem. Soc.* **2009**, *131*, 2615−2620.

(14) Bediako, D. K.; Costentin, C.; Jones, E. C.; Nocera, D. G.; Savéant, J.-M. Proton−Electron Transport and Transfer in Electrocatalytic Films. Application to a Cobalt-Based O$_2$-Evolution Catalyst. *J. Am. Chem. Soc.* **2013**, *135*, 10492−10502.

(15) Klingan, K.; Ringleb, F.; Zaharieva, I.; Heidkamp, J.; Chernev, P.; Gonzalez-Flores, D.; Risch, M.; Fischer, A.; Dau, H. Water Oxidation by Amorphous Cobalt-Based Oxides: Volume Activity and Proton Transfer to Electrolyte Bases. *ChemSusChem* **2014**, *7*, 1301−1310.

(16) González-Flores, D.; Sánchez, I.; Zaharieva, I.; Klingan, K.; Heidkamp, J.; Chernev, P.; Menezes, P. W.; Driess, M.; Dau, H.; Montero, M. L. Heterogeneous Water Oxidation: Surface Activity versus Amorphization Activation in Cobalt Phosphate Catalysts. *Angew. Chem.* **2015**, *127*, 2502−2506.

(17) Risch, M.; Ringleb, F.; Kohlhoff, M.; Bogdanoff, P.; Chernev, P.; Zaharieva, I.; Dau, H. Water Oxidation by Amorphous Cobalt-Based Oxides: In Situ Tracking of Redox Transitions and Mode of Catalysis. *Energy Environ. Sci.* **2015**, *8*, 661−674.

(18) Risch, M.; Klingan, K.; Heidkamp, J.; Ehrenberg, D.; Chernev, P.; Zaharieva, I.; Dau, H. Nickel-oxido Structure of a Water-oxidizing Catalyst Film. *Chem. Commun.* **2011**, *47*, 11912−11914.

(19) Bediako, D. K.; Lassalle-Kaiser, B.; Surendranath, Y.; Yano, J.; Yachandra, V. K.; Nocera, D. G. Structure-activity Correlations in a Nickel-borate Oxygen Evolution Catalyst. *J. Am. Chem. Soc.* **2012**, *134*, 6801−6809.

(20) Bediako, D. K.; Surendranath, Y.; Nocera, D. G. Mechanistic Studies of the Oxygen Evolution Reaction Mediated by a Nickel−Borate Thin Film Electrocatalyst. *J. Am. Chem. Soc.* **2013**, *135*, 3662−3674.

(21) Dincă, M.; Surendranath, Y.; Nocera, D. G. Nickel-Borate Oxygen-Evolving Catalyst That Functions under Benign Conditions. *Proc. Natl. Acad. Sci. U. S. A.* **2010**, *107*, 10337−10341.

(22) Singh, A.; Chang, S. L. Y.; Hocking, R. K.; Bach, U.; Spiccia, L. Anodic Deposition of NiOx Water Oxidation Catalysts from Macrocyclic Nickel(ii) Complexes. *Catal. Sci. Technol.* **2013**, *3*, 1725−1732.

(23) Singh, A.; Chang, S. L. Y.; Hocking, R. K.; Bach, U.; Spiccia, L. Highly Active Nickel Oxide Water Oxidation Catalysts Deposited from Molecular Complexes. *Energy Environ. Sci.* **2013**, *6*, 579−586.

(24) Wang, D.; Ghirlanda, G.; Allen, J. P. Water Oxidation by a Nickel-Glycine Catalyst. *J. Am. Chem. Soc.* **2014**, *136*, 10198−10201.

(25) Hoang, T. T. H.; Gewirth, A. High Activity Oxygen Evolution Reaction Catalysts from Additive-Controlled Electrodeposited Ni and NiFe Films. *ACS Catal.* **2016**, *6*, 1159−1164.

(26) Lu, C.; Wang, J.; Chen, Z. Water Oxidation by Copper−Amino Acid Catalysts at Low Overpotentials. *ChemCatChem* **2016**, *8*, 2165−2170.

(27) Yu, F.; Li, F.; Zhang, B.; Li, H.; Sun, L. Efficient Electrocatalytic Water Oxidation by a Copper Oxide Thin Film in Borate Buffer. *ACS Catal.* **2015**, *5*, 627−630.

(28) Li, T.-T.; Cao, S.; Yang, C.; Chen, Y.; Lv, X.-J.; Fu, W.-F. Electrochemical Water Oxidation by In Situ-Generated Copper Oxide Film from [Cu(TEOA)(H$_2$O)$_2$][SO$_4$] Complex. *Inorg. Chem.* **2015**, *54*, 3061−3067.

(29) Wang, T.; LaMontagne, D.; Lynch, J.; Zhuang, J.; Cao, Y. C. Colloidal Superparticles from Nanoparticle Assembly. *Chem. Soc. Rev.* **2013**, *42*, 2804−2823.

(30) Min, Y.; Akbulut, M.; Kristiansen, K.; Golan, Y.; Israelachvili, J. The Role of Interparticle and External Forces in Nanoparticle Assembly. *Nat. Mater.* **2008**, *7*, 527−538.

(31) Grzelczak, M.; Vermant, J.; Furst, E. M.; Liz-Marzán, L. M. Directed Self-Assembly of Nanoparticles. *ACS Nano* **2010**, *4*, 3591−3605.

(32) Wang, L.; Xu, L.; Kuang, H.; Xu, C.; Kotov, N. A. Dynamic Nanoparticle Assemblies. *Acc. Chem. Res.* **2012**, *45*, 1916−1926.

(33) Shenhar, R.; Norsten, T. B.; Rotello, V. M. Polymer-Mediated Nanoparticle Assembly: Structural Control and Applications. *Adv. Mater.* **2005**, *17*, 657−669.

(34) Yamanoi, Y.; Yamamoto, Y.; Miyachi, M.; Shimada, M.; Minoda, A.; Oshima, S.; Kobori, Y.; Nishihara, H. Nanoparticle Assemblies via Coordination with a Tetrakis(terpyridine) Linker Bearing a Rigid Tetrahedral Core. *Langmuir* **2013**, *29*, 8768−8772.

(35) Martis, M.; Mori, K.; Fujiwara, K.; Ahn, W.-S.; Yamashita, H. Amine-Functionalized MIL-125 with Imbedded Palladium Nanoparticles as an Efficient Catalyst for Dehydrogenation of Formic Acid at Ambient Temperature. *J. Phys. Chem. C* **2013**, *117*, 22805−22810.

(36) Takashima, T.; Hashimoto, K.; Nakamura, R. Mechanisms of pH-dependent Activity for Water Oxidation to Molecular Oxygen by $MnO_2$ Electrocatalysts. *J. Am. Chem. Soc.* **2012**, *134*, 1519−1527.

(37) Yoshida, M.; Mineo, T.; Mitsutomi, Y.; Yamamoto, F.; Kurosu, H.; Takakusagi, S.; Asakura, K.; Kondoh, H. Structural Relationship between $CoO_6$ Cluster and Phosphate Species in a Cobalt-Phosphate Water Oxidation Catalyst Investigated by Co and P K-edge XAFS. *Chem. Lett.* **2016**, *45*, 277−279.

(38) Nakaoka, K.; Ueyama, J.; Ogura, K. Semiconductor and Electrochromic Properties of Electrochemically Deposited Nickel Oxide Films. *J. Electroanal. Chem.* **2004**, *571*, 93−99.

(39) Nakaoka, K.; Ogura, K. Electrochemical Preparation of p-type Cupric and Cuprous Oxides on Platinum and Gold Substrates from Copper (II) Solutions with Various Amino Acids. *J. Electrochem. Soc.* **2002**, *149*, C579−C585.

(40) Ogura, K.; Nakaoka, K.; Nakayama, M.; Tanaka, S. A New Type of Electrochemical Formation of Copper Oxide during Redox Processes of the Copper(II)−Glycine Complex at High pH. *J. Electroanal. Chem.* **2001**, *511*, 122−127.

(41) Yoshida, M.; Mitsutomi, Y.; Mineo, T.; Nagasaka, M.; Yuzawa, H.; Kosugi, N.; Kondoh, H. Direct Observation of Active Nickel Oxide Cluster in Nickel−Borate Electrocatalyst for Water Oxidation by In Situ O K-Edge X-ray Absorption Spectroscopy. *J. Phys. Chem. C* **2015**, *119*, 19279−19286.

(42) Chen, J. G. NEXAFS Investigations of Transition Metal Oxides, Nitrides, Carbides, Sulfides and Other Interstitial Compounds. *Surf. Sci. Rep.* **1997**, *30*, 1−152.

(43) Zubavichus, Y.; Zharnikov, M.; Schaporenko, A.; Grunze, M. NEXAFS Study of Glycine and Glycine-based Oligopeptides. *J. Electron Spectrosc. Relat. Phenom.* **2004**, *134*, 25−33.